Accurate Optical Detection of Amphiphiles at Liquid-Crystal–Water Interfaces

Piotr Popov,[1] Elizabeth K. Mann,[1] and Antal Jákli[2,*]

[1]*Department of Physics, Kent State University, Kent, Ohio 44240, USA*

[2]*Liquid Crystal Institute, Kent State University, Kent, Ohio 44240, USA*

(Received 17 December 2013; revised manuscript received 30 January 2014; published 15 April 2014)

Liquid-crystal–based biosensors utilize the high sensitivity of liquid-crystal alignment to the presence of amphiphiles adsorbed to one of the liquid-crystal surfaces from water. They offer inexpensive, easy optical detection of biologically relevant molecules such as lipids, proteins, and cells. Present techniques use linear polarizers to analyze the alignment of the liquid crystal. The resulting images contain information not only about the liquid-crystal tilt with respect to the surface normal, the quantity which is controlled by surface adsorption, but also on the uncontrolled in-plane liquid-crystal alignment, thus making the detection largely qualitative. Here we show that detecting the liquid-crystal alignment between circular polarizers, which are only sensitive to the liquid-crystal tilt with respect to the interface normal, makes possible quantitative detection by measuring the transmitted light intensity with a spectrophotometer. Following a new procedure, not only the concentration dependence of the optical path difference but also the film thickness and the effective birefringence can be determined accurately. We also introduce a new "dynamic" mode of sensing, where (instead of the conventional "steady" mode, which detects the concentration dependence of the steady-state texture) we increase the concentration at a constant rate.

DOI: 10.1103/PhysRevApplied.1.034003

I. INTRODUCTION

Liquid crystals (LCs) combine the long-range orientational order and fluidity that makes them the first choice in the multibillion-dollar information display technology [1]. Because of the long-range orientational order [2], LCs can transmit such order at a surface into the bulk, which results in a change of the average liquid-crystal molecular orientation (director) with respect to the surface [3] that can be easily detected optically via the change of effective birefringence. This property provides a quick and easy way of detecting extremely small amounts of surface molecules that affect the liquid-crystal alignment [4–9]. Surfactant-decorated LC surfaces have been developed to detect competitive binding of cholic acid [10], specific enzymatic reactions [11–13], bacterial catalase interactions [14], heavy metals [15,16], DNA hybridization [17], and DNA interaction with immobilized oligonucleotides [18]. Additionally, 4'-pentyl-4-cyanobiphenyl (5CB) laden with polyacrylic acid block liquid-crystalline polymers have been used to detect proteins [19]. Specific binding of vesicles has been studied at liquid-crystal interfaces laden with proteins [20]. Specific antibody interaction with surface antigen immobilized at a LC interface has been used for detection of hepatitis B immunocomplex [21].

Surfactants usually promote the alignment of the LC director parallel to the surfactant chains and, thus, on average, normal to the substrate (homeotropic), whereas water promotes tangential (planar) alignment. A water-LC interface is, therefore, very sensitive to the presence of surfactants, such as the phospholipids that are found in biological membranes. This sensitivity is the principle of the LC-based chemical and biological sensing technique introduced by Abbott and co-workers [8,12,22]. This technique consists of a nematic liquid-crystal film suspended in a grid, with one LC interface locked into homeotropic alignment by a substrate and one interface exposed to the aqueous solution [Fig. 1(a)]. The change in the transmission of polarized light through the cell due to the realignment at the aqueous interface and the subsequent reconfiguration of the bulk LC provides an easily read signal. Transmission electron microscope (TEM) grids made of gold, copper, or nickel with a thickness of about 20 μm and a mesh size of a few hundred micrometers provide a convenient, readily available support. Typically, one interface of the grid filled with a nematic liquid crystal is in contact with a solid substrate that promotes homeotropic alignment, whereas the other interface is in contact with water, which, in the absence of surfactants, promotes planar alignment [Fig. 1(a)]. Most of the previous studies used the well-known liquid crystal 5CB and the homeotropic alignment coating octadecyltrichlorosilane (OTS), although, recently, a wider range of liquid crystals and alignment coatings have been tested also [23]. The LC interface with air also promotes homeotropic anchoring, and, thus, a sensor with air replacing the solid homeotropic alignment layer has been tested recently [11]. The advantage of using air as a substrate is that air very consistently reproduces homeotropic alignment at any level of humidity,

*Corresponding author.
ajakli@kent.edu

while the quality of alignment at a solid substrate must be carefully controlled [11,24]. The textural changes in bulk LC induced by the interaction of the LC at the aqueous interface can be easily detected optically using polarizing optical microscopy (POM). The transmitted light through a LC slab between crossed linear polarizers is sensitive to both the LC director tilt with respect to the surface normal and to the LC in-plane orientation. The transmitted light intensity is given by the following formula [25]:

$$I(\lambda) = I_0 \times \frac{1}{2} \times \sin^2(2\varphi) \times \sin^2\left(\frac{\pi}{\lambda} \times \Delta n \times d\right), \qquad (1)$$

where φ is the angle between the local in-plane LC director orientation and the light polarization direction, d is the thickness of the LC slab, Δn is the effective birefringence which is given by the LC director tilt with respect to the surface normal, λ is the wavelength of the light, and I_0 is the intensity of the incoming unpolarized light.

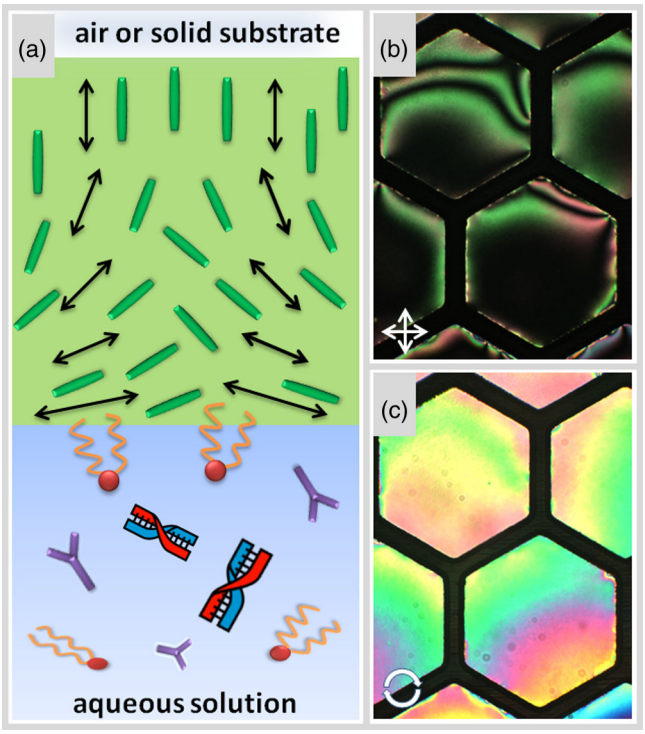

FIG. 1. Illustration of the principle of liquid-crystal-based biosensors. (a) Cross section of two possible evolutions of the liquid-crystal director (arrows) consistent with the boundary conditions imposed by air above and the aqueous solution below. Any configuration with this same structure at an arbitrary angle with respect to the plane of the figure is also consistent with the boundary conditions. (b) Typical texture of the liquid crystal in a TEM grid seen between crossed linear polarizers (polarization directions illustrated by white arrows). (c) Texture of the liquid crystal in the TEM grid seen between the left and right circular polarizers (indicated by white circle). The diameter of the hexagonal cells is 0.5 mm.

Water imposes random planar orientation: the two LC configurations illustrated in Fig. 1(a) yield the same $I(\lambda)$ under crossed linear polarizers, while configurations rotated by an angle 1°–44° with respect to the plane of the figure are all equally likely and give different $I(\lambda)$. Indeed, the tangential component of the director changes spatially, as can be seen in the typical "brushes" observed in Fig. 1(b). The darkest regions correspond to $\sin^2(2\varphi) = 0$, while the brightest regions correspond to $\sin^2(2\varphi) = 1$. Usually, one averages $I(\lambda)$ over a large number of cells, assuming completely random planar orientation, but flow and other unwanted factors impose some partial and unpredictable orientation. This makes the observations at best semiquantitative and requires large surface areas. Typically, only an average intensity $I(\lambda)$ is measured through an average gray level, which restricts the observations to the range where the effective birefringence is small so that $\Delta n \times d/\lambda \ll 1$. In sum, the use of linear polarizers mixes information on the relevant LC director tilt with respect to the surface normal with information on the irrelevant component along the interface. The irrelevant information impedes the quantitative analysis of the influence of the biomolecule of interest.

The substitution of circular polarizers for linear ones selects the information of interest for diagnosing the presence and conformation of molecules at the LC surface [Fig. 1(c)]. Like linear polarizers, circular polarizers have also been widely used in optical applications, such as in photography to eliminate unwanted glare [26] and in 3D glasses to produce stereoscopic effects in movies that support the 3D technology [27]. In combination with linear polarizers, they also have been used in photoelasticity measurements of transparent solid materials [28,29]. They also have been utilized in LC-based microsensors to detect localized changes in the spatial distribution of pointlike tracers [30], although, to the best of our knowledge, so far they have not been used to determine the global orientation in LC-based sensors.

The transmitted intensity $I(\lambda)$ between the left and right circular polarizers is

$$I(\lambda) = I_0 \times \sin^2\left(\frac{\pi}{\lambda} \times \Delta n \times d\right), \qquad (2)$$

which does not depend on φ, so it does not contain information about the uncontrolled azimuthal orientation of the LC director, as can be seen in Fig. 1(c).

This paper studies the liquid-crystal orientation in response to surfactants with a pair of left and right circular polarizers. We show that the use of circular polarizers eliminates the need of averaging over large areas and separate detection in each cell in the grid becomes possible. In addition to this simple but important change, we also demonstrate that measuring the spectral distribution $I(\lambda)$ with a spectrophotometer allows quantitative and accurate

determination of the retardation of the LC sensor. Finally, by combining measurements for three different interfacial conditions, the film thickness and the effective birefringence can be determined separately. We test this sensor against three representative types of molecules: an anionic surfactant, a nonionic surfactant, and a phospholipid. This approach and methodology offers a wide range of applications in chemical and biological sensors.

II. MATERIALS AND METHODS

The chemical structures of the materials and the picture of the TEM grid held by tweezers used in this study are shown in Figs. 2(a) and 2(b). The room temperature nematic liquid crystal is 5CB. For surfactants, nonionic tetra(ethylene glycol)monooctyl ether (C_8E_4) and ionic sodium dodecyl sulfate (SDS) are used and obtained from Sigma Aldrich (St. Louis, MO). We also study a biologically more relevant phospholipid, 1,2-dilauroyl-sn-glycero-3-phosphocholine (DLPC) from Avanti Polar Lipids, Inc. All chemicals are used without further purification.

The water we use in all experiments is purified using a PureLab Plus system (18.2 MΩ cm). We purchase copper square 75 mesh and nickel hexagonal 50/100 mesh Veco folding TEM grids from Ted Pella, Inc. Both types of grids are 20 μm thick and have a diameter of 3.05 mm.

A 35-mm glass-bottom microscope dish from Azzota holds the solution. Before each experiment, the TEM grid and microscope dish are cleaned in hexane and then in methanol with an ultrasonic cleaner (Branson B200). In all measurements, the TEM folding grid contains two twin halves as shown in Fig. 2(b). One of the halves ("sensing part") is required for hosting the sensing LC, while the other one ("holding part") is simply used for holding by tweezers. The sensing part is adjusted to be parallel to the solution surface by rotating the holding part until the sensing area can be focused uniformly. The LC suspended in the grid is found to be stable for weeks either in water or in air. The water always stays in contact with the LC because it is pinned on the rim of the metallic grid, as illustrated in Fig. 2(c). Because of this pinning, the level of the water may vary up to 5 mm without losing contact with the LC. The rate of increase of the surfactant concentration due to the water evaporation is found to be negligible during the sensing measurements.

To measure the birefringence, the liquid-crystal film suspended in the TEM grids is illuminated with a collimated white light, and the wavelength dependence of the transmitted light intensity is measured with an Ocean

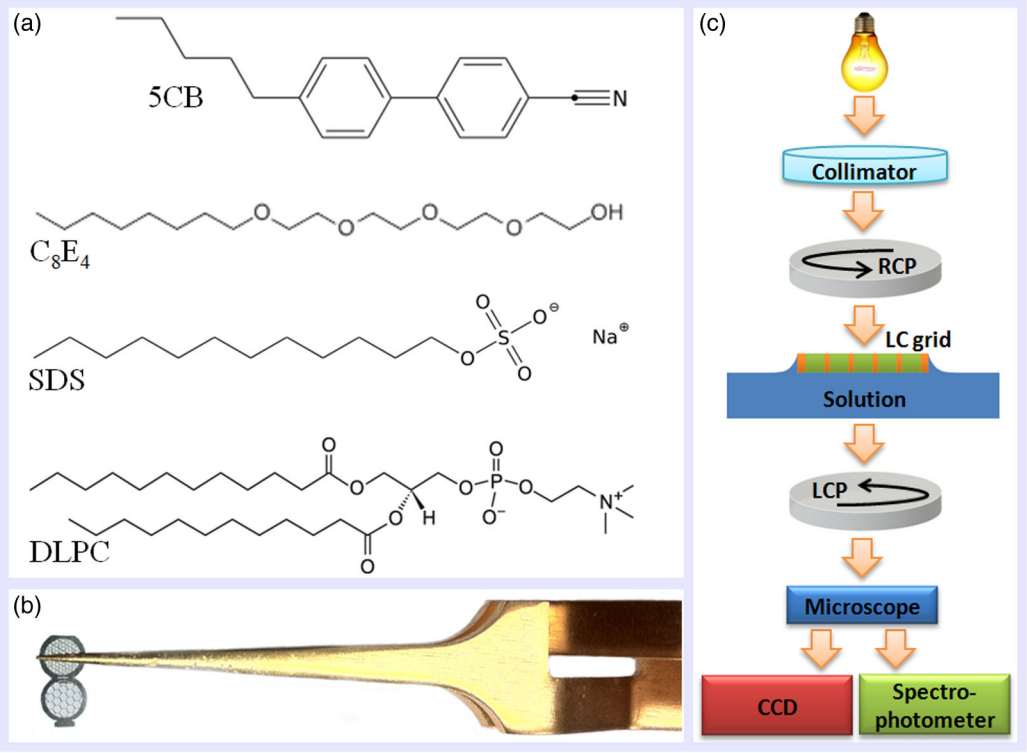

FIG. 2. Chemical structures of the materials and sketches of the experimental setup. (a) Molecular structures of the sensing liquid crystal 5CB, a nonionic detergent C_8E_4, an ionic detergent SDS, and a phospholipid DLPC. (b) Image of the folding grids held by tweezers. (c) Sketch of the experimental setup including the light beam, circular polarizers, water with surfactant in contact with the TEM grid supporting the sensing LC, and the detections using a CCD camera and an OceanOptics spectrophotometer.

Optics HR2000 + spectrophotometer. The transmittance $\sin^2(\pi \times \Delta n \times d/\lambda)$ shows maxima and minima when $\Delta n \times d/\lambda = 1/2 + m$ and $\Delta n \times d/\lambda = m$ (where m is a positive integer), respectively. Provided we know the film thickness, we obtain Δn by measuring the wavelengths of the maxima and minima. The larger the number of maxima and minima, the larger the birefringence; we can determine Δn at all maxima and minima, which gives information about the wavelength dependence of the birefringence (dispersion) $\Delta n(\lambda)$ of the material.

As the birefringence decreases, the number of maxima and minima decreases, too, but we can still get Δn at smaller wavelengths from the position of a maximum or minimum as long as there is at least one. For the $d = 20$ μm film, the lowest value of the birefringence that we can get from the position of the last maximum is $\Delta n_m = 0.4/(2 \times 20) = 0.01$. When $\Delta n < \Delta n_m$, one should compare the transmitted light intensity to that at maxima using Eq. (2).

For such low birefringence values, it is particularly critical to know the parasitic light intensity (light leakage), which may arise from slight deviations from normal incidence, from alignment defects at the boundary of the grid and from nonperfect polarizers. The effect of parasitic light is minimized by the following procedure: First, light is collected from the center of a single grid cell, as shown in Figs. 3 and 4. The transmitted light intensity is measured in the presence of the LC cell in contact with air at both interfaces, providing homeotropic alignment which is dark either between the left and right circular polarizers or between the crossed linear polarizers. This signal is saved as the dark state signal D_λ. Then the top polarizer is removed so that all of the light goes through the homeotropically aligned 5CB. This signal is saved as a bright reference state R_λ. The resulting signal S_λ is then transformed to the percent transmission T_λ by the formula

$$T_\lambda = \frac{S_\lambda - D_\lambda}{R_\lambda - D_\lambda} \times 100\%. \tag{3}$$

This transmission is then used to determine the birefringence and its dispersion relation.

Based on these considerations, all measured T_λ spectra are fitted by the formula

$$I(\lambda) = I_0 \times \sin^2\left(\frac{\pi}{\lambda} \times \frac{\Delta n(\lambda) \times d}{S}\right) + I_p, \tag{4}$$

in which I_0 is the incoming light intensity, α, β, γ are the Cauchy coefficients for dispersion of the nematic LCs,

$$\Delta n(\lambda) = \alpha + \frac{\beta}{\lambda^2} + \frac{\gamma}{\lambda^4}, \tag{5}$$

I_p is the additional parasitic light intensity, and S is a scaling parameter. For 5CB, $\alpha = 0.1569$, $\beta = 0.0029$ μm^2, and $\gamma = 0.0016$ μm^4 according to Li *et al.* [31]. The parameter S scales the 5CB birefringence depending on the angle between the LC director and the LC-water interface plane:

$$\Delta n_{\text{eff}}(\lambda) = \frac{\Delta n(\lambda)}{S}. \tag{6}$$

In Eq. (4), the variable is the wavelength λ, the fitting parameters are I_0, I_p, S, and α, β, γ, d are held fixed. The scaling parameter is introduced to reduce the number of fitting parameters and improve the stability of this nonlinear fit. It assumes that the dispersion does not change with variations in molecular tilt through the cell.

The measured $I(\lambda)$ gives the birefringence only if we know the film thickness; it is crucial to determine the film thickness precisely. This is difficult, because the thickness

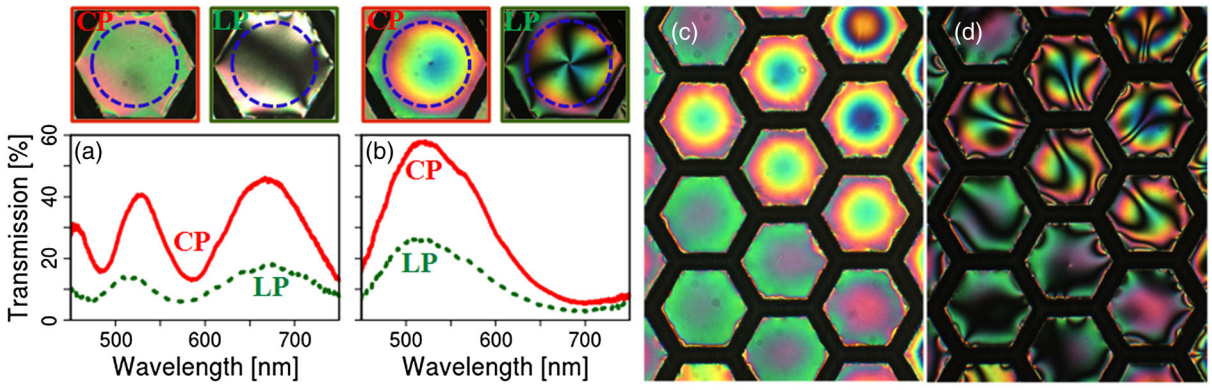

FIG. 3. Comparison of transmission signals obtained when using linear crossed polarizers (green dashed curve and right cell both marked with LP) and circular polarizers (red solid curve and left cell both marked with CP) with water and air interfaces. (a) An evenly filled cell. (b) An underfilled cell exhibiting interference rings due to a meniscus. (c) Texture of a cell array between circular polarizers. (d) Texture of a cell array between crossed linear polarizers. The diameter of the hexagonal cells is 0.5 mm. Spectrophotometer measurement is collected only from within the dashed blue circles and not from entire cells.

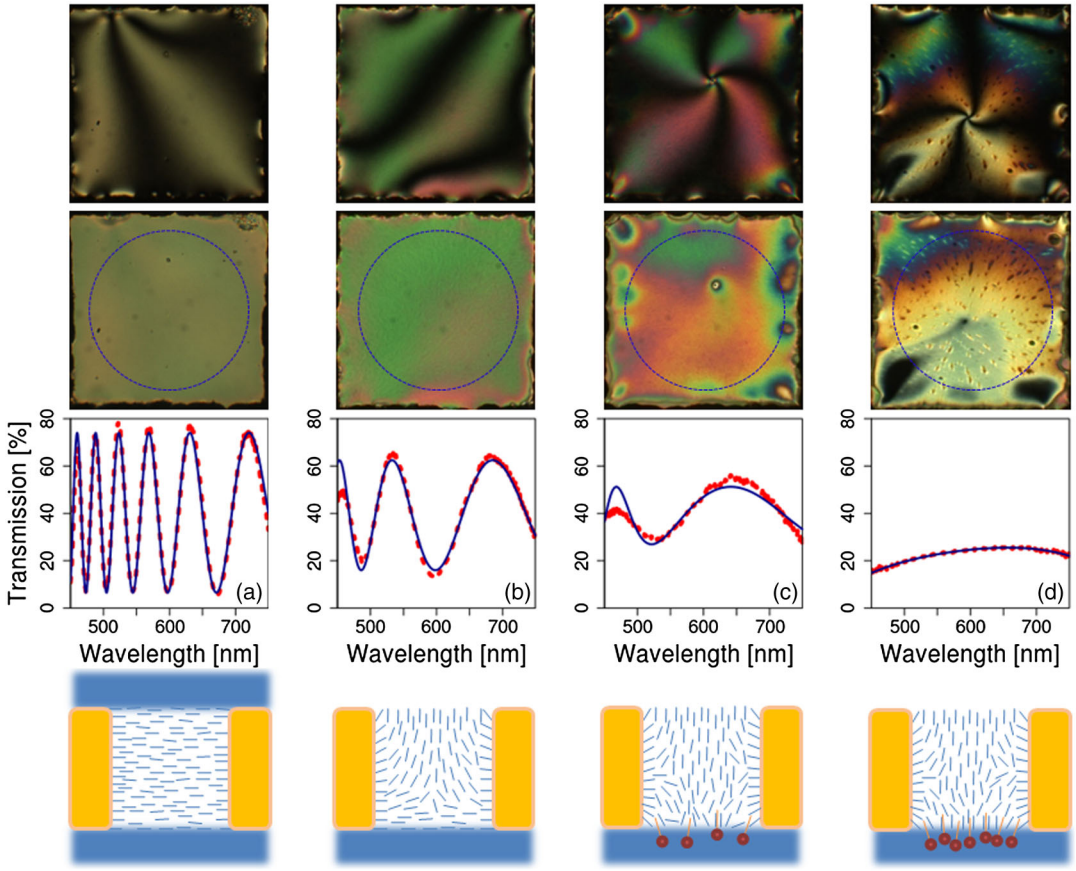

FIG. 4. Illustration of optical textures, the wavelength dependence of transmitted intensities between circular polarizers in different LC-water-air-surfactant combinations. The size of the square cell is 250 μm. Top row: Textures between crossed linear polarizers. Second row: Textures between circular polarizers. Spectrophotometer measurement is collected only from within the dashed blue circles and not from the entire cell. Third row: Wavelength dependences of the transmitted intensities measured on single cells between circular polarizers together with the nonlinear fit using Eq. (4). Bottom row: Illustration of the substrateless configurations. (a) Water-water interfaces using $S = 1$ and finding $d = 23.53 \pm 0.02$ μm. (b) Water and air interfaces $S = 2.355 \pm 0.001$. (c) Solution ($C = 2.5$ mM C_8E_4) and air interfaces $S = 4.298 \pm 0.008$. (d) Solution ($C = 4.5$ mM C_8E_4) and air interfaces $S = 12.58 \pm 0.04$.

of the grid can vary and because the grids can be underfilled or overfilled. The first case usually leads to a variation of the film thickness; the liquid crystal wets the grid causing a meniscus. As we will discuss, this can easily be identified by the spatial variation of the birefringent color. However, it is also possible that the liquid crystal can have an extra layer that spans the entire film including the grid area. This results in uniform birefringence, which cannot be identified by the varying birefringence color and leads to an overestimate of the birefringence. To exclude this error, we also measure $I(\lambda)$ when the cell is completely immersed underwater, which orients 5CB molecules parallel to the interface, so $\Delta n_{\text{eff}} = \Delta n$, i.e., $S = 1$. Therefore, the fit to Eq. (4) with $S = 1$ is used to accurately determine the film thickness d, which was observed not to change when the upper layer of water evaporates and the surfactant is added to the lower layer of water. By this procedure, therefore, we are able to measure Δn_{eff} accurately.

III. EXPERIMENTAL RESULTS

Figure 3 shows the textures and the corresponding wavelength dependence of the transmitted light intensities seen in between the linear and circular polarizers. Figure 3(a) compares the textures and the wavelength dependence of the transmitted light intensity for a well-filled individual cell. The texture seen between the circular polarizers is fairly uniform with a green birefringence color, whereas the same area looks inhomogeneous with dark brushes when viewed between the crossed linear polarizers. The corresponding spectra show the maxima and minima at the same wavelengths (indicating nearly the same birefringence), but the intensity is much larger between the circular polarizers. Figure 3(b) shows the textures and the corresponding transmission spectra for one example of an underfilled grid. In this case, a centered defect line with strength $+1$ with four brushes is seen between the linear polarizers, but it appears only as a small dark dot between the circular

polarizers. In addition, the images with the circular polarizers show circular rings with decreasing birefringence colors, revealing that the thickness of the liquid crystal decreases toward the center of the grid. The appearance of defects is uncontrolled, and they do not always appear when the circular meniscus rings are present, as evidenced by the top-right images of Figs. 3(c) and 3(d). Films without a meniscus provide a determination of the cell thickness in the water-water case, following the procedure above. A correct value of the effective birefringence can be readily determined from the data in Fig. 3(a), while the data from Fig. 3(b) first require that we determine the thickness distribution. It is much less time consuming to simply choose cells without a meniscus.

In the air-air mode, when 5CB molecules are arranged perpendicular (homeotropic) with respect to the grid plane, the texture appears homogenously black across the entire cell, except at the boundaries of the grid; the LC molecules within several microns of the boundary are mostly aligned parallel to the grid plane. Gold, nickel, and copper grids are all found to produce this short-range homeotropic anchoring. It is important to emphasize that the measured spectra are not collected from the entire cell area. The inner diameter of the hexagonal cell is 0.43 mm, while only the area of a circle with diameter of approximately 0.4 mm is used to collect the spectra, as shown in Figs. 3 and 4 by the dashed blue circles. In this way, it is possible to avoid the light leakage that comes from the anchoring of LC to the metal grid.

Figures 3(c) and 3(d) show a number of cells between the circular and linear polarizers, respectively. The images with circular polarizers in Fig. 3(c) show some cells (in the bottom-left of the image, about $1/3$ of the whole area) that exhibit circular ring patterns indicating they are underfilled. We observe that this large percentage of underfilled cells is quite typical even when one side of the film is in contact with air, and it becomes even worse in the traditional homeotropic substrate and water configuration because during immersion underwater, some of the LC tends to wash away. This illustrates the importance of identifying and excluding underfilled cells from the birefringence measurements to achieve precise sensing.

In Fig. 4, we compare the textures between the crossed linear polarizers (top row) and between the circular polarizers (second row) and show the wavelength dependences of the transmitted intensities measured between the circular polarizers by using Eq. (3) together with the nonlinear fit using Eq. (4) (third row) in four different configurations illustrated in the bottom row. Figure 4(a) represents a cell that is completely immersed underwater. As explained above, here we set $S = 1$ in Eq. (6) to obtain an accurate value of the film thickness, which presumably will not change upon the evaporation of the top water layer. Although it is rare, due to the hydrophobic nature of the thermotropic LC, underfilled cells with ring pattern may appear, as seen in Fig. 3(b) and in the top corner of Figs. 3(c) and 3(d). Ring patterns never develop during the experiment but only at the moment when the LC is filled into the grid or at the moment of complete immersion into water, suggesting that once formed, the film thickness remains constant in time.

In Fig. 4(b), the cell is in contact with water at the bottom (planar alignment) and with air on top (homeotropic alignment). This results in a hybrid alignment exhibiting a smaller effective birefringence, which is evidenced by the reduced number of maxima (3) and minima (2). The scaling parameter for Cauchy coefficients is $S = 2.355 \pm 0.001$. The situations when 2.5 and 4.5-mM surfactant C_8E_4 are added to the water are shown in Figs. 4(c) and 4(d), respectively. As evidenced by the decreased number of maxima [two for Fig. 4(c) and one for Fig. 4(d)] and minima [one for Fig. 4(c) and zero for Fig. 4(d)], the birefringence further decreases upon addition of surface-active molecules to the water. In spite of the small number of extrema, the scaling parameters can be still determined from the fitting Eq. (4). The scaling parameter in Fig. 4(c) is $S = 4.298 \pm 0.008$, and it is further increased in Fig. 4(d) to $S = 12.58 \pm 0.04$ due to the C_8E_4 increased concentration.

The dark brushes that appear even at zero surfactant concentrations in between the crossed linear polarizers are due to the azimuthal orientation of the director either parallel or perpendicular to the linear polarizers, as evidenced by the uniform birefringence color seen between the circular polarizers. This demonstrates the advantage of the circular polarizers. Additionally, they are easier to use, since they do not need to be precisely oriented with respect to each other, in contrast to linear polarizers that need to be set perpendicular to each other. The inhomogeneous areas seen in between the circular polarizers in the second row of Fig. 4 are steady at a given concentration, thus, indicating inhomogeneous surfactant distribution. The reasons for this inhomogeneous distribution are unclear, but their nature depends strongly on the surfactant, its concentration, and addition history; these would be interesting to study further.

Figure 5 qualitatively compares the effect of C_8E_4 [the critical micelle concentration (CMC) = 8.5 mM] nonionic surfactant with the ionic SDS (CMC = 8.2 mM). Although the induced textures seen by POM are very similar, the concentration ranges are very different; about 6 times more C_8E_4 is needed to drive the hybrid geometry completely into a homeotropic state. Since the CMC values for both surfactants are almost the same, we attribute this difference to a better affinity to 5CB of SDS compared to C_8E_4.

In Fig. 6, we show the results of quantitative birefringence measurements using the circular polarizers of the water-air system for the surfactant SDS added to the water. In Fig. 6(a), the wavelength-dependent effective birefringences are plotted with standard deviation bands. Similar to

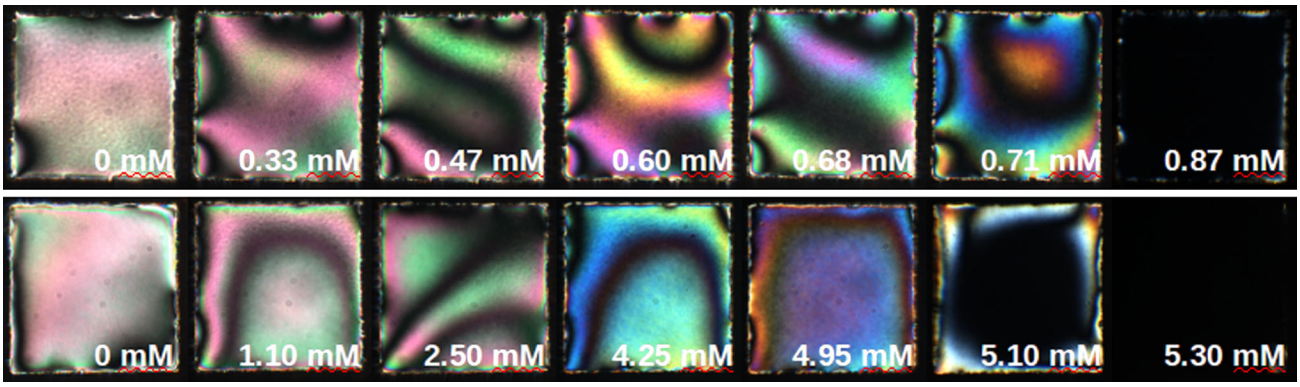

FIG. 5. Comparison of the effect of SDS and C_8E_4 on the alignment of the liquid crystal 5CB. Top row: Ionic surfactant, SDS. Bottom row: Nonionic surfactant, C_8E_4. Textures are obtained using linear crossed polarizers.

the observation shown in Fig. 4, we find that the dispersion decreases with increasing concentration. We also see that the standard deviation increases toward higher concentrations, because the number of peaks decreases and the fit becomes less sensitive. Figure 6(b) shows the dependence of the SDS concentration on the effective birefringences at three wavelengths. As the concentration increases, the effective birefringence decreases, and the dispersion vanishes. The typical textures seen between the circular polarizers are also shown in Fig. 6(b). The results are consistent with the work reported by Iglesias *et al.* [23] in the sense that the SDS concentration needed to switch to homeotropic state is the same, but the birefringence values are slightly higher here. This is partially due to the lower homeotropic anchoring energy at the LC-air interface than at the LC-polymer interface used in an earlier study and partially because here we have averaged the effective birefringence only over carefully selected cells and not the entire grid.

The dynamics of the sensor and, in particular, the time to reach equilibrium of surface-active molecules with the LC-solution interface, depends on the concentration of the surfactant: the lower the concentration, the more time is needed. For this reason, although typically a 30-min waiting time is sufficient, the data points of Fig. 6(b) are obtained after a 60-min waiting time. With insufficient waiting time, the graph in Fig. 6(b) will exhibit a plateau for low surfactant concentration and the biosensor will be regarded as insensitive in that range.

Although the response time of a LC-based biosensor can be shortened by either decreasing the thickness of the LC films or by increasing the temperature, in some cases, it still

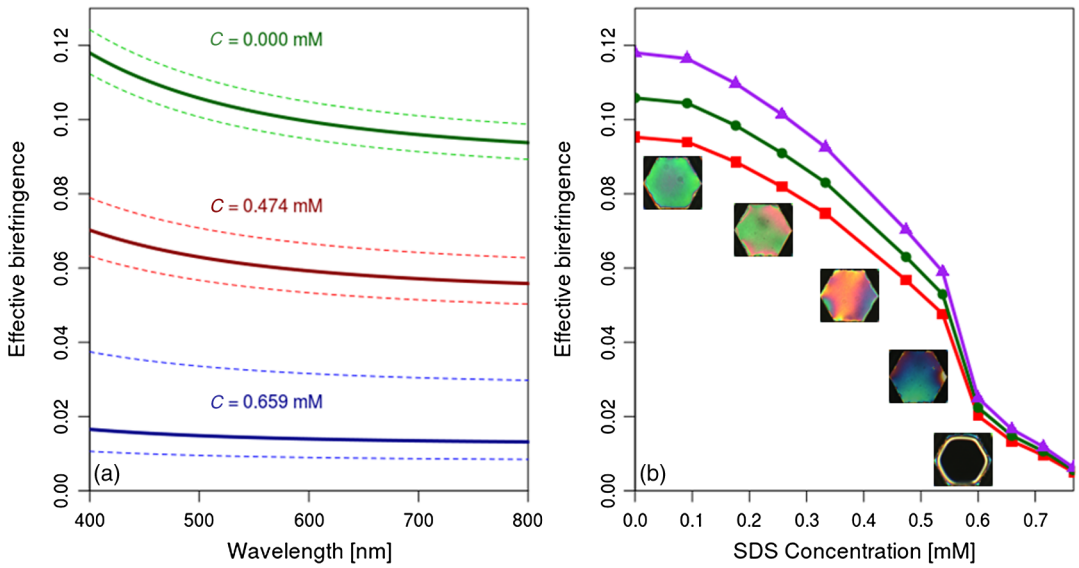

FIG. 6. (a) Solid curves: Effective birefringence dispersion of 5CB bounded by air and solution at different SDS concentrations. The curves are plotted with dashed uncertainty bands. (b) Effective birefringence vs SDS concentration for different wavelengths with textures obtained using circular polarizers. Red curve with squares 650 nm, green curve with circles 510 nm, purple with triangles 400 nm. These measurements are obtained in an experiment using six individual cells.

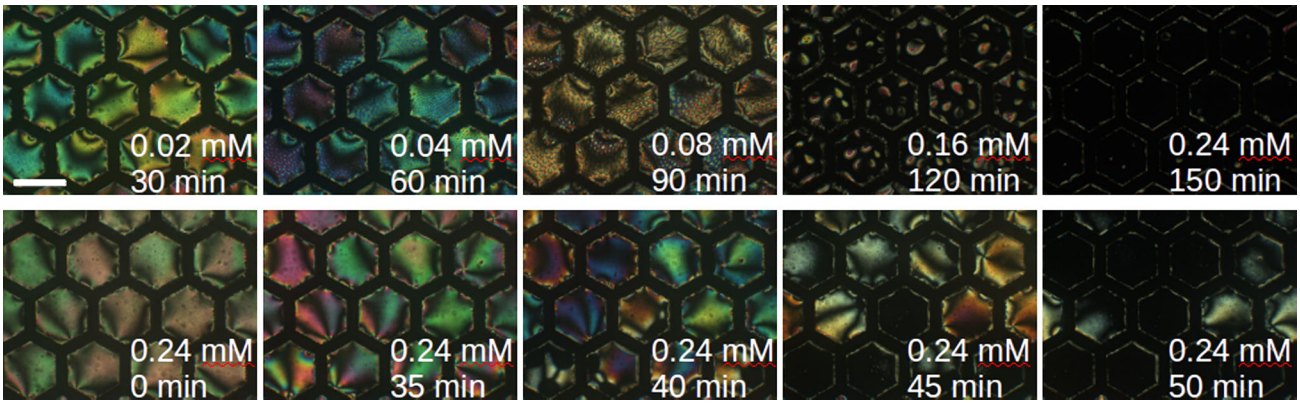

FIG. 7. Demonstration of a dynamic mode of sensing DLPC phospholipid. Top row: Slow incremental rate of lipid concentration. Bottom row: Lipid concentration is initially high and held constant. The bar represents 0.5 mm.

can be too slow. For example, in case of the phospholipid DLPC (CMC = 90 n*M*), even the lowest 0.02-m*M* concentration we use is about 200 times higher than the critical micelle concentration of the DLPC. The director orientation transitions completely to the homeotropic state given enough time, but this transition takes about one day. For this reason, instead of studying the concentration dependence after very long waiting times, we study the concentration dependence of the texture (and birefringence) after constant (30 min) increments of waiting times. The qualitative POM results are shown in the top row of Fig. 7. The texture changes by the nucleation and growth of domains when the lipid concentration is increased slowly and reaches the dark state only at a 0.24-m*M* concentration. When we add DLPC at a 0.24-m*M* concentration initially, no nucleating domains appear and the texture becomes uniformly darker with time, reaching a nearly homeotropic state in about 50 min (see Fig. 7 bottom row). These clear differences between the different concentrations indicate that, depending on the dynamics and concentration range of the surfactant, one may use the LC-based biosensor in a "steady" mode, which was studied by Kinsinger *et al.* by depositing the lipid Langmuir monolayers at a fixed density [32], or switch to a "dynamic" mode, where the sensing range depends on the rate of the concentration change. A fast rate can distinguish between large concentrations with low concentrations hardly registering, while a slow rate can distinguish between low concentrations with higher ones saturating the signal. For very small amphiphile concentrations, one should change the concentration at a low rate, while for larger concentrations, a higher rate can be used. The introduction of this new dynamic mode, therefore, allows setting the range of the sensitivity, although further studies are needed to fully utilize the capabilities of this mode.

In summary, we demonstrate two features of LC-based sensors: (i) More precise measurements can be done even on single grid cells if we use left and right circular polarizers instead of the traditional crossed linear polarizers; this opens up the possibility of multiplexing by varying the LC or surface composition from cell to cell. (ii) Using circular polarizers makes possible, if desired, a new measurement procedure which gives not only the optical path difference $\Delta n_{\mathrm{eff}} d$ but separately both Δn_{eff} and d, thus, allowing more surfactants to be distinguished. Note that in some cases, linear polarizers can give interesting additional information, for example, when one is interested in defect structure and dynamics.

In addition to the conventional static mode in which the steady-state birefringence is monitored as a function of the surfactant concentration, one may use a dynamic mode in which the concentration is changed at a constant rate, and the time dependence of the birefringence is used to measure the concentration of the surfactant. This way, not only the concentration-dependent birefringence but also the time dependence of the birefringence can be used to specify the type of the surfactant we want to sense.

ACKNOWLEDGMENTS

This work is supported by NSF Grant No. DMR-0907055. We acknowledge useful discussions with N. Abbott at University of Wisconsin-Madison and P. Bos at Liquid Crystal Institute of Kent State University.

[1] H. Kawamoto, The history of liquid-crystal displays, Proc. IEEE **90**, 460 (2002).
[2] J. D. Parsons, Nematic ordering in a system of rods, Phys. Rev. A **19**, 1225 (1979).
[3] B. J. Zywucki and W. Kuczynski, The orientational order in nematic liquid crystals from birefringence measurements, IEEE Trans. Dielectr. Electr. Insul. **8**, 512 (2001).
[4] M. J. Uline, S. Meng, and I. Szleifer, Surfactant driven surface anchoring transitions in liquid crystal thin films, Soft Matter **6**, 5482 (2010).
[5] Y. Dong and Z. Yang, Beyond displays: The recent progress of liquid crystals for bio/chemical detections, Chin. Sci. Bull. **58**, 2557 (2013).

[6] A. Hussain, A. S. Pina, and A. C. A. Roque, Bio-recognition and detection using liquid crystals, Biosens. Bioelectron. **25**, 1 (2009).

[7] A. D. Price and D. K. Schwartz, Fatty-acid monolayers at the nematic/water interface: Phases and liquid-crystal alignment, J. Phys. Chem. B **111**, 1007 (2007).

[8] R. J. Carlton, J. T. Hunter, D. S. Miller, R. Abbasi, P. C. Mushenheim, L. N. Tan, and N. L. Abbott, Chemical and biological sensing using liquid crystals, Liq. Cryst. Rev. **1**, 29 (2013).

[9] M. K. McCamley, M. Ravnik, A. W. Artenstein, S. M. Opal, S. Žumer, and G. P. Crawford, Detection of alignment changes at the open surface of a confined nematic liquid crystal sensor, J. Appl. Phys. **105**, 123504 (2009).

[10] S. He, W. Liang, C. Tanner, K. -L. Cheng, J. Fang, and S.-T. Wu, Liquid crystal based sensors for the detection of cholic acid, Anal. Methods **5**, 4126 (2013).

[11] D. Hartono, X. Bi, K.-L. Yang, and L.-Y. L. Yung, An air-supported liquid crystal system for real-time and label-free characterization of phospholipases and their inhibitors, Adv. Funct. Mater. **18**, 2938 (2008).

[12] J. M. Brake, M. K. Daschner, Y.-Y. Luk, and N. L. Abbott, Biomolecular interactions at phospholipid-decorated surfaces of liquid crystals, Science **302**, 2094 (2003).

[13] X. Bi, D. Hartono, and K. -L. Yang, Real-time liquid crystal pH sensor for monitoring enzymatic activities of penicillinase, Adv. Funct. Mater. **19**, 3760 (2009).

[14] Q.-Z. Hu and C.-H. Jang, Using liquid crystals for the label-free detection of catalase at aqueous-LC interfaces, J. Biotechnol. **157**, 223 (2012).

[15] Q.-Z. Hu and C.-H. Jang, Liquid crystal–based sensors for the detection of heavy metals using surface-immobilized urease, Colloids Surf. B **88**, 622 (2011).

[16] S. Yang, C. Wu, H. Tan, Y. Wu, S. Liao, Z. Wu, G. Shen, and R. Yu, Label-free liquid crystal biosensor based on specific oligonucleotide probes for heavy metal ions, Anal. Chem. **85**, 14 (2013).

[17] A. D. Price and D. K. Schwartz, DNA hybridization-induced reorientation of liquid crystal anchoring at the nematic liquid crystal/aqueous interface, J. Am. Chem. Soc. **130**, 8188 (2008).

[18] S. L. Lai, S. Huang, X. Bi, and K.-L. Yang, Optical imaging of surface-immobilized oligonucleotide probes on DNA microarrays using liquid crystals, Langmuir **25**, 311 (2009).

[19] J.-M. Seo, W. Khan, and S.-Y. Park, Protein detection using aqueous/LC interfaces decorated with a novel polyacrylic acid block liquid crystalline polymer, Soft Matter **8**, 198 (2012).

[20] L. N. Tan, V. J. Orler, and N. L. Abbott, Ordering transitions triggered by specific binding of vesicles to protein-decorated interfaces of thermotropic liquid crystals, Langmuir **28**, 6364 (2012).

[21] C.-H. Chen and K.-L. Yang, Liquid crystal–based immunoassays for detecting hepatitis B antibody, Anal. Biochem. **421**, 321 (2012).

[22] S. J. Woltman, G. D. Jay, and G. P. Crawford, Liquid-crystal materials find a new order in biomedical applications, Nat. Mater. **6**, 929 (2007).

[23] W. Iglesias, N. L. Abbott, E. K. Mann, and A. Jákli, Improving liquid-crystal-based biosensing in aqueous phases, ACS Appl. Mater. Interfaces **4**, 6884 (2012).

[24] V. Nazarenko and A. Nych, Multistable alignment in free suspended nematic liquid crystal films, Phys. Rev. E **60**, R3495 (1999).

[25] A. Jakli and A. Saupe, *One-and Two-Dimensional Fluids: Properties of Smectic, Lamellar and Columnar Liquid Crystals* (Taylor & Francis, Boca Raton, FL, 2006), pp. 163–166.

[26] E. Fariza, E. A. Jalkh, V. J. Thomas, T. O'Day, E. Peli, and J. Acosta, Use of circularly polarized light in fundus and optic disc photography, Arch. Ophthalmol. **106**, 1001 (1988).

[27] K. Iizuka, Three-dimensional camera phone, Appl. Opt. **43**, 6285 (2004).

[28] K. Ramesh, *Digital Photoelasticity* (Springer, New York, 2000).

[29] A. Shukla, High-speed fracture studies on bimaterial interfaces using photoelasticity—a review, J. Strain Anal. Eng. Des. **36**, 119 (2001).

[30] E. Brasselet and S. Juodkazis, Intangible pointlike tracers for liquid-crystal-based microsensors, Phys. Rev. A **82**, 063832 (2010).

[31] J. Li, C.-H. Wen, S. Gauza, R. Lu, and S.-T. Wu, Refractive indices of liquid crystals for display applications, J. Disp. Technol. **1**, 51 (2005).

[32] M. I. Kinsinger, D. M. Lynn, and N. L. Abbott, Nematic ordering drives the phase separation of mixed monolayers containing phospholipids modified with poly(ethylene glycol) at aqueous–liquid crystal interfaces, Soft Matter **6**, 4095 (2010).